Neutron and proton spectra from the decay of Λ hypernuclei

A. Ramos

Departament d'Estructura i Constituents de la Matèria, Universitat de Barcelona, 08028 Barcelona, Spain

M.J. Vicente-Vacas and E. Oset

Departamento de Física Teórica and IFIC, Centro Mixto Universidad de Valencia-CSIC, 46100 Burjassot, Valencia, Spain

Abstract

We have determined the spectra of neutrons and protons following the decay of Λ hypernuclei through the one- and two-nucleon induced mechanisms. The momentum distributions of the primary nucleons are calculated and a Monte Carlo simulation is used to account for final state interactions. From the spectra we calculate the number of neutrons (N_n) and protons (N_p) per Λ decay and show how the measurement of these quantities, particularly N_p, can lead to a determination of Γ_n/Γ_p, the ratio of neutron to proton induced Λ decay. We also show that the consideration of the two-nucleon induced channel has a repercussion in the results, widening the band of allowed values of Γ_n/Γ_p with respect to what is obtained neglecting this channel.

I. INTRODUCTION

The apparent discrepancy between the ratio of the $\Lambda n \to nn$ and $\Lambda p \to np$ cross sections predicted by the one pion exchange model (OPE) [1–3] and experiments looking at neutrons and protons from the decay of Λ hypernuclei [4–6], has stimulated much theoretical work, refining the OPE model with the addition of the exchange of other mesons [2,7], using correlated two pion exchange [8,9], or considering quark degrees of freedom [10,11]. In spite of these efforts, no theoretical approach leads, without ambiguities, to values of Γ_n/Γ_p of the order of unity, as claimed by experiment, compared to values of the order of 0.1 that one obtains in the OPE model. Before proceeding further one should, however, notice that the experimental errors are very large [5,6].

Some hopes for the understanding of the large fraction of neutrons observed in the experiment were raised in Ref. [12], where the two-nucleon (2N) induced Λ decay was studied. Indeed, in this latter mechanism a near on-shell pion is produced in the $\Lambda N\pi$ vertex and the pion is then absorbed mostly by a neutron-proton pair. Hence, one has the reaction $\Lambda np \to nnp$ and two neutrons and one proton are emitted in this process, while in the one-nucleon (1N) induced Λ decay processes ($\Lambda p \to np$, $\Lambda n \to nn$), a np or nn pair is produced. Thus, even if the $\Lambda n \to nn$ process was suppressed, as in the OPE model, one could still have a large fraction of neutrons produced if one had a sizable Λ decay width through the 2N induced channel.

The idea of Ref. [12] was reanalyzed and the calculations improved in Ref. [13] with the surprising result that the consideration of the 2N induced channel, in connection with the measured number of neutrons and protons, led to ratios of Γ_n/Γ_p even larger than those extracted before and in worse agreement with the OPE results. These conclusions, however, were based on the assumption that all the emitted particles were detected.

On the other hand, it was pointed out that, in case only two particles from the $\Lambda NN \to NNN$ reaction were detected, the analysis of the data with the consideration of the 2N induced Λ decay channel would lead to smaller values of Γ_n/Γ_p [14].

These findings indicate that the values obtained for Γ_n/Γ_p are sensitive to the detection thresholds for nucleons and, hence, a precise determination of Γ_n/Γ_p requires a theoretical calculation of the nucleon spectra coming from the different mechanisms. Furthermore, a precise comparison with the experimental spectra requires also to address the problem of the final state interactions of the nucleons on their way out of the nucleus.

The aim of the present paper is to evaluate the energy spectra for protons and neutrons, coming from the different mechanisms, as functions of Γ_n/Γ_p, which will be treated as an unknown. Hence, comparison of the experimental neutron and proton spectra with the theoretical predictions, or even just the number of neutrons and protons emitted per Λ decay, would allow to determine the ratio Γ_n/Γ_p.

II. DETERMINATION OF THE INITIAL NUCLEON SPECTRA

In order to determine the neutron and proton spectra we use the formalism of Refs. [13,15] for the 1N and 2N induced Λ decay, which uses the local density approximation to evaluate the width of finite Λ hypernuclei starting from the self-energy of a Λ particle in infinite nuclear matter.

The mesonic Λ decay can also be treated in this way [15], but the sensitivity to the nuclear and pion wave functions makes the finite nucleus treatment more accurate [16–19]. In any case, there is no need to consider the nucleons emitted in the mesonic decay since their energy is around 5 MeV, which lies below any of the ordinary detection thresholds. One may still wonder about secondary nucleons coming from pionic Λ decay at some point in the nucleus with a subsequent absorption of this pion on its way out of the nucleus. However, the pions produced in the pionic Λ decay have an energy of around 20—30 MeV and they are weakly absorbed in the nucleus. Moreover, due to Pauli blocking, these pions will be mainly produced at the surface and, consequently, they will be even less absorbed. From the analogous (γ,π) reaction in ^{12}C we can see that less than 10% of the 25 MeV primary produced pions are later on absorbed (compare $\sigma_{\rm abs}$ and $\sigma_{\rm dir\,abs}$ of Fig. 8 in Ref. [20]). Since

the mesonic width is $\Gamma_m = 0.3\Gamma_\Lambda$ for ${}^{12}_{\Lambda}$C, where Γ_Λ is the free Λ width, then the fraction of reabsorbed pions would be about 3% of Γ_Λ or, equivalently, less than 2% of the total Λ width in ${}^{12}_{\Lambda}$C [5]. This is a negligible amount and would be further reduced in heavier nuclei since Γ_m decreases very fast with the mass of the hypernucleus.

The preceding discussion allows us to consider only the nucleons coming from the 1N and 2N induced Λ decay. The local density formalism of Refs. [13,15] is particularly suited to treat the final state interaction of the nucleons since these are produced at a certain point in the nucleus and with a certain momentum. Then we can follow these nucleons by means of a Monte Carlo computer simulation which takes into account quasielastic nucleon collisions, pion production, etc. The accuracy of this procedure to deal with nucleon propagation in the nucleus was established in Ref. [21], by comparing some results with the corresponding full Quantum Mechanical ones.

Recalling the results of [13,15] we write the decay width of a hypernucleus as

$$\Gamma = \int d^3k \tilde{\rho}(\mathbf{k}) \Gamma(\mathbf{k}) \ , \tag{1}$$

with

$$\Gamma(\mathbf{k}) = \int d^3r |\psi_\Lambda(\mathbf{r})|^2 \Gamma(\mathbf{k}, \rho(\mathbf{r})) \ ,$$

where $\psi_\Lambda(\mathbf{r})$ is the Λ wave function in the nucleus and $\rho(\mathbf{r})$ the nuclear density. The former equations show that $\Gamma(\mathbf{k})$ is evaluated by means of the local density approximation and Γ is then obtained by weighing $\Gamma(\mathbf{k})$ with the momentum distribution of the Λ in nucleus, $\tilde{\rho}(\mathbf{k})$. The weighing over $\mathbf{k}$ is more important in the evaluation of the mesonic decay width for heavy nuclei but has little relevance in the nonmesonic decay width which we study here, since $\Gamma(\mathbf{k})$ is rather smoothly dependent on $\mathbf{k}$ for this channel. However, keeping the $\mathbf{k}$ dependence becomes again relevant for the distribution of momenta of the emitted nucleons.

The nuclear matter width, $\Gamma(\mathbf{k}, \rho)$, is evaluated from the Λ self-energy via the equation

$$\Gamma = -2 Im \, \Sigma \tag{2}$$

where Σ accounts for the diagrams of Figs. 1 and 2. As shown in Refs. [13,15] the resulting width is

$$\Gamma(\mathbf{k},\rho) = -6(G\mu^2)^2 \int \frac{d^3q}{(2\pi)^3}[1-n(\mathbf{k}-\mathbf{q})]\theta(k^0 - E(\mathbf{k}-\mathbf{q}) - V_N)$$
$$\times\, Im\,\alpha(q)|_{q^0=k^0-E(\mathbf{k}-\mathbf{q})-V_N} \tag{3}$$

with

$$\alpha(q) = \left(S^2 + \left(\frac{P}{\mu}\right)^2 \mathbf{q}^2\right) F^2(q) D_0(q)$$
$$+ \frac{\tilde{S}^2(q)\overline{\Pi}^*(q)}{1 - V_L(q)\overline{\Pi}^*(q)} + \frac{\tilde{P}_L^{\,2}(q)\overline{\Pi}^*(q)}{1 - V_L(q)\overline{\Pi}^*(q)} + 2\frac{\tilde{P}_T^2(q)\overline{\Pi}^*(q)}{1 - V_T(q)\overline{\Pi}^*(q)}\ , \tag{4}$$

where $\alpha(q)$ is related to the dressed pion propagator and accounts for the effect of short range NN and ΛN correlations. The explicit expressions for $\tilde{S}, \tilde{P}_L, \tilde{P}_T$ are defined in Eqs. (20), (23), and (24) of Ref. [15] (denoted there by C', B', A' respectively). In Eqs. (3) and (4), the quantities $E(\mathbf{p})$ and V_N stand for the nucleon energy, $\sqrt{\mathbf{p}^2 + M^2}$, and potential energy, respectively, $F(q)$ is the πNN form factor, $n(\mathbf{p})$ the nucleon occupation number of a noninteracting Fermi system of density ρ, $D_0(q)$ the free pion propagator, and V_L (V_T) the longitudinal (transverse) part of the spin-isospin ph interaction. The function $\overline{\Pi}^*$, related to the pion self-energy through

$$\Pi^*(q) = \frac{f^2}{\mu^2}\mathbf{q}^2 F^2(q)\overline{\Pi}^*(q)\ , \tag{5}$$

is given by

$$\overline{\Pi}^* = \overline{\Pi}^*_{\rm 1p1h} + \overline{\Pi}^*_{\Delta\rm h} + \overline{\Pi}^*_{\rm 2p2h}\,, \tag{6}$$

and accounts for particle-hole (1p1h), delta-hole (Δh) and two particle-two hole (2p2h) excitation. Furthermore, $\overline{\Pi}^*_{\rm 1p1h} = U_N$ and $\overline{\Pi}^*_{\Delta\rm h} = U_\Delta$ are the ordinary Lindhard functions for 1p1h and Δh excitation [22], with the normalization of the appendix of Ref. [3]. On the other hand, $\overline{\Pi}^*_{\rm 2p2h}$ is constructed in Ref. [13] from data of p-wave pion absorption in pionic atoms, extrapolated for pions off shell by means of the phase space for real 2p2h excitation. In Eq. (3) we have $Im\,\alpha(q)$ which, as one can see from Eq. (4), contains the free pion propagator and other terms which renormalize the pion in the medium. As noted in Ref.

[13], the sum of the longitudinal terms from $Im\,\alpha(q)$ in Eq. (4) leads to a peak around the position of the renormalized pion in the medium, with a width given by

$$\Gamma_\pi(q) = -\frac{1}{\tilde{\omega}(q)} Im\,\Pi(\tilde{\omega}(q), q)\ , \tag{7}$$

where Π is the pion proper self-energy and $\tilde{\omega}(q)$ the renormalized pion energy in the medium. The proper self-energy Π is related to $\overline{\Pi}^*$ by means of

$$\Pi(q^0, q) = \frac{\Pi^*(q^0, q)}{1 - \frac{f^2}{\mu^2} g'(q) \overline{\Pi}^*(q^0, q)} \tag{8}$$

with g' the Landau-Migdal parameter (smoothly q dependent). For the pions emitted in the Λ decay, $Im\,\Pi$ in Eq. (8) is actually $Im\,\Pi_{\rm 2p2h}$, since there is no strength from $Im\,\Pi_{\rm 1p1h}$ at the pion pole and furthermore $Im\,U_\Delta$ is practically zero there. One must then be cautious interpreting the strength coming from $Im\,\overline{\Pi}^*_{\rm 2p2h}$ as due to 2p2h excitation, since part of it belongs to the excitation of the renormalized pion, which contributes to the mesonic channel. In heavy nuclei, where the pionic decay mode is practically forbidden by Pauli blocking, this association is clear, but in light and medium nuclei, where there is still a certain fraction of mesonic decay, one must do the separation of the mesonic and 2p2h channels. On the other hand, the 1p1h channel offers no problems because it does not mix with the pion pole term. Thus, the strength coming from Eq. (3), obtained by substituting in $Im\,\alpha(q)$

$$Im\,\frac{\overline{\Pi}^*(q)}{1 - V_{L,T}(q)\overline{\Pi}^*(q)} \rightarrow \frac{Im\,\overline{\Pi}^*_{\rm 1p1h}(q)}{|1 - V_{L,T}(q)\overline{\Pi}^*(q)|^2} \tag{9}$$

and omitting the $D_0(q)$ term, corresponds to 1p1h excitation.

In Ref. [13] the strength of the 2p2h excitation was obtained by subtracting from the whole width, calculated with the full $Im\,\alpha(q)$, the contribution of the mesonic and the 1p1h excitation channels. The mesonic channel was calculated with the zero width approximation at the position of the renormalized pion pole and the 1p1h excitation channel was obtained with the procedure indicated in Eq. (9).

In the present work we have adopted a more practical procedure which leads to the same results. The strength around the renormalized pion pole has been omitted by cutting $Im\,\alpha(q)$

between $\tilde{\omega} - \lambda\Gamma_\pi$ and $\tilde{\omega} + \lambda\Gamma_\pi$, with $\lambda = 0.8$, a value that has been adjusted to reproduce the same 2p2h width as that obtained in Ref. [13]. This eliminates the contribution of the mesonic channel and leaves only those of the 1p1h and the 2p2h excitation channels. After this cut is done, the part of Γ in Eq. (3) proportional to $Im\,\overline{\Pi}^*_{\rm 1p1h}$, through Eq. (9), and the analogous one proportional to $Im\,\overline{\Pi}^*_{\rm 2p2h}$ are now associated to the 1N induced and 2N induced Λ decay, respectively.

The evaluation of the final nucleon momenta proceeds in two steps. First, we determine the distribution of momenta after the Λ decay (primary step). Next, we consider the final state interactions of the nucleons via a Monte Carlo simulation, which will be discussed in the next section.

In order to determine the primary nucleon momenta let us look at the structure of the integrals involved in the evaluation of Γ

$$\Gamma_i = \int d^3k \int d^3r \int d^3q \ldots Im\,\overline{\Pi}^*_i(q^0 = k^0 - E(\mathbf{k}-\mathbf{q}) - V_N, q) \ , \tag{10}$$

with the index i standing for 1p1h or 2p2h, or alternatively, 1N and 2N induced mechanisms. On the other hand, we have from Fig. 3a

$$Im\,\overline{\Pi}^*_{\rm 1p1h}(q^0, q) \ \propto \int d^3p\, n(\mathbf{p})[1 - n(\mathbf{p}+\mathbf{q})]\delta(q^0 + E(\mathbf{p}\,) - E(\mathbf{p}+\mathbf{q})) \ , \tag{11}$$

which can be further simplified eliminating the δ function. Furthermore, from Fig. 3b we have

$$\begin{aligned} Im\,\overline{\Pi}^*_{\rm 2p2h}(q^0, q) \propto \int d^4k'\, Im\,U_N(\frac{q}{2} + k', \rho) Im\,U_N(\frac{q}{2} - k', \rho) \\ \times\, \theta(\frac{q^0}{2} + k'^{\,0})\theta(\frac{q^0}{2} - k'^{\,0}) \ , \end{aligned} \tag{12}$$

which can be further simplified as shown in Ref. [13].

In the 1p1h mechanism, a change of variables in Eq. (11) can be performed leaving the momentum of the emitted nucleon, $\mathbf{p}+\mathbf{q}$, as integration variable. In the 2p2h case, each of the Lindhard functions appearing in Eq. (12) involves an integration over an internal hole momentum, $\mathbf{p}_{h_1}$ and $\mathbf{p}_{h_2}$, respectively. As for the previous case, a change of integration

variables in terms of the two emitted nucleon momenta ($\mathbf{q}/2+\mathbf{k}'+\mathbf{p}_{h_1}$ and $\mathbf{q}/2-\mathbf{k}'+\mathbf{p}_{h_2}$) can be made. Then, one can perform the integrations using the Monte Carlo method, since the integrands are smooth once the pion peak is removed. Each configuration point generated by the Monte Carlo technique corresponds to a set of momenta for the outgoing primary nucleons.

In the evaluation of the 1p1h and 2p2h induced Λ decay widths we have followed Ref. [13] and the 1p1h induced channel is evaluated using the OPE model. This could give a poor description of the Γ_n/Γ_p ratio, but so far, the different attempts to improve on this ratio discussed in the Introduction share one feature in common, which is that the decay rate is barely changed with respect to that obtained with the OPE model. Hence, we keep the probability obtained by the OPE model for the 1p1h channel fixed, and take the ratio Γ_n/Γ_p as a variable. For the same reason, we also keep the nucleon momentum distribution provided by the OPE model. A pure phase space calculation gives a very similar shape for the momentum distributions.

III. MONTE CARLO SIMULATION

In this section we show how the charge selection and the propagation of the nucleons is done with the Monte Carlo simulation. We follow closely the steps developed in the study of inclusive pionic reactions [23], in (γ,π) reactions in nuclei [20] and in $(\gamma,N),(\gamma,NN),(\gamma,N\pi)$ photonuclear reactions [21].

In the first place a random number is generated which decides whether we have a 1N induced event or a 2N induced one, according to their respective probabilities. Next we determine the momenta of the primary nucleons emitted in the decay process. This is done by generating random configurations which are weighted by their corresponding probability according to the model described in the previous section. This gives us the momenta of nucleon 1 and nucleon 2 in Fig. 4, for the 1N induced mechanism, and nucleons 1, 2, 3 in Fig. 5 for the 2N induced mechanisms.

Next we determine the charge of the particles. In Figs. 4 and 5 we show diagrammatically the neutron and protons which would come out from the 1p1h and 2p2h mechanisms. In the case of the 1N induced process we generate a random number which decides whether we have $\Lambda n \to nn$ or $\Lambda p \to np$, according to the probability Γ_n/Γ_p, which we keep as a free parameter in the theory. In the case of $\Lambda n \to nn$, each neutron is given one of the momenta corresponding to nucleon 1 and nucleon 2 in Fig. 4a. In the case of $\Lambda p \to np$ (Fig. 4b) we associate also random, with equal probability, the n and p to nucleons 1 and 2 and viceversa. With all these random decissions one has now an event corresponding to a pair of nucleons, pn or nn, with some definite momenta.

If the event was a 2N induced one (Fig. 5), then we decide by means of a random number whether one has the mechanism of Fig. 5a or the one of Fig. 5b, taking into account that the one of Fig. 5b has a probability twice as large as the mechanism of Fig. 5a. In the case of the mechanism of Fig. 5a one still has to do a further decission, which is whether to place pn in numbers 2,3 or viceversa. This is also decided random giving the same weight to the two possibilities (as would come out in a model of absorption dominated by the Δ excitation in the πN vertex [24]). However, in this case this last step has no consequences since the distribution of nucleons 2 and 3 is symmetrical from Eq. (12).

With the former steps we have selected a configuration for a primary event. One of the variables in the Monte Carlo integration is $\mathbf{r}$, the vector position in the nucleus where the Λ decay takes place. Hence, each event in the Monte Carlo integration determines the point at which the primary nucleons are produced and this allows us to follow the fate of these nucleons on their way out of the nucleus. This is done by allowing the nucleons to undergo collisions with other nucleons of the nucleus according to NN cross sections, modified by Pauli blocking and polarization phenomena. The method is detailed in Ref. [21], where a useful parametrization of the cross sections borrowed from Ref. [25] is also shown.

In the Monte Carlo simulation the nucleons emitted in the decay are allowed to move through the nucleus under the influence of a local potential given by the Thomas Fermi model, $V_N(r) = -k_F(r)^2/2M$. As the nucleons move out of the nucleus they collide with

the nucleons of the local Fermi sea. In the collisions the nucleons change energy, direction and, eventually, charge since the differencial cross sections used for pn collisions allow configurations in which a fast proton colliding with a neutron of the Fermi sea gives rise to a fast neutron and a slowly moving proton. In each collision, a nucleon from the Fermi sea is excited above the local Fermi momentum and the propagation of this secondary unbound nucleon, which has an energy larger than its mass, must also be followed. Eventually, each primary nucleon may produce several nucleons that leave the nucleus. At the end, we know the energy and direction of each one of the emitted protons and neutrons, be primary or secondary nucleons.

IV. RESULTS AND DISCUSSION

In Fig. 6 we show the spectrum of neutrons and protons coming from the 1N and 2N induced mechanisms in the decay of ${}^{12}_{\Lambda}$C, assuming a value $\Gamma_n/\Gamma_p = 1$. Hence, as can be inferred from Fig. 4 for the 1N induced mechanisms, one expects three times more neutrons than protons at each energy if one neglects the effect of final state interaction and charge exchange. By comparing the dotted line (neutrons) with the dashed line (protons), we can see that this is approximately the case, except at low energies where mostly secondary nucleons show up. The kinetic energy peaks around 70 MeV and there is a broad peak which reflects the Fermi motion of the nucleons and the Λ momentum distribution. In the same figure, the spectrum of neutrons (dash-dotted line) and protons (solid line) coming from the 2N induced mechanism is also shown. In this case, the distribution is rather flat, since three particles are involved in the initial and final state and both Fermi motion and the final phase space collaborate in producing the broadening of the spectrum. At large energies we find that there are about four times more neutrons than protons. This indicates that the nucleons appearing at this high energy region are mainly those generated from the absorption of the virtual pion (nucleons 2 and 3 in Figs. 5a and 5b). In fact, if only the two nucleons coming from the absorption of the virtual pion contributed to this part of the

spectrum, we would have found five times more neutrons than protons. However, although the nucleons coming from de Λ vertex are in general slow, there is a tail at large energies which lowers the ratio. On the other hand, we also observe in Fig. 6 a peak with about the same number of neutrons as protons at low energies around 10 MeV. These nucleons come mostly from the Λ decay vertex and from final state interaction effects. We should note, however, that at energies around and below 20 MeV our spectra are not realistic. The semiclassical Monte Carlo procedure becomes progressively less reliable at low energies and other phenomena like evaporation etc., not considered by us, would come into play. However, this is of minor importance here since ordinary experimental detection thresholds are higher than this energy.

The effect of final state interactions (FSI) can be seen by comparing the solid lines with the dashed lines in Fig. 7. We observe that FSI affect mostly the nucleon distributions at energies below 40 MeV. Only a small fraction of the neutrons and protons at large energies is removed due to FSI, whereas, at energies below 40 MeV, strength from both the degradation of the primary nucleons and the emission of secondary nucleons is collected.

As a complementary information we show in Fig. 8 the spectrum of protons from the 1N (dotted line) and 2N (dashed line) induced mechanisms, calculated with a value $\Gamma_n/\Gamma_p = 0.1$. The solid line is the total proton spectrum. The features of the spectra are similar to those in Fig. 6 although the number of protons or neutrons per Λ decay emitted in one case or the other is obviously rather different. For this reason we discuss below these magnitudes as functions of Γ_n/Γ_p.

In the first place, we show in Figs. 9 and 10 the ratio of the number of emitted neutrons to that of emitted protons per Λ decay, N_n/N_p, as a function of Γ_n/Γ_p, omitting FSI and assuming, respectively, that all particles are observed or that a threshold cut of 40 MeV is applied in the detection energy. The idea behind these curves is to facilitate the determination of the ratio Γ_n/Γ_p from the measured N_n/N_p ratio.

We observe that the resulting N_n/N_p ratio increases with the value of Γ_n/Γ_p, but the results depend on whether we consider only the 1N induced mechanism (dashed line) or we

include also the 2N induced one (solid line). In Fig. 9 we observe that, for a value of $\Gamma_n/\Gamma_p = 0.5$, the ratio N_n/N_p is the same whether one considers the 1N induced mechanism only or both mechanisms. However, given an experimental value of N_n/N_p, the corresponding value of Γ_n/Γ_p including the 2N induced decay is bigger than the one obtained considering only the 1N induced mechanism if $\Gamma_n/\Gamma_p > 0.5$. The situation is reversed if $\Gamma_n/\Gamma_p < 0.5$. This is exactly the result obtained analytically in Ref. [13]. However, if a cut of 40 MeV in the detection energy is applied, as can be seen in Fig. 10, the point where the two curves cross appears at larger values of Γ_n/Γ_p (in the figure at $\Gamma_n/\Gamma_p = 1.3$). As follows from the discussions above in connection with Fig. 6, a cut of 40 MeV would eliminate mostly the peak corresponding to the nucleons emitted from the Λ vertex. Therefore, the results in Fig. 10 follow the tendency indicated in Ref. [14], where it is shown that, if the nucleon from the Λ vertex is not observed, the two lines in the figure would cross at a value of $\Gamma_n/\Gamma_p = 2$.

In Fig. 11 we show results including FSI and taking threshold energy cuts of 0, 30 and 40 MeV. The last two cases allow to compare our results with the measurements of Ref. [5]. The numbers found there, corrected as indicated in Ref. [13,26], were $N_n^{\rm TOT} = N_0 N_n = 3400 \pm 1100$, $N_p^{\rm TOT} = N_0 N_p = 1270 \pm 180$, for $E_{\rm cut} = 30$ MeV and $N_n^{\rm TOT} = 2530 \pm 1050$, $N_p^{\rm TOT} = 1112 \pm 130$, for $E_{\rm cut} = 40$ MeV, where N_0 is the total number of decay events. From the results shown in Fig. 11 we can deduce that the band of allowed values of $N_n^{\rm TOT}/N_p^{\rm TOT} = N_n/N_p$ corresponds to values of Γ_n/Γ_p in the range 0.15—2.0 for $E_{\rm cut} = 30$ MeV and 0.0—1.65 for $E_{\rm cut} = 40$ MeV. It is important to note that these results are even compatible with the OPE predictions. We should also point out that the inclusion of the 2N induced channel enlarges the band of allowed values at both ends, with respect to the results which would be obtained omitting this channel. One can also see that the effect of the 2N induced channel becomes smaller for higher threshold detection energies, as can be easily understood from the fact that the average energy of the nucleons in the 2N induced channel is smaller than in the 1N induced one.

The information contained in Fig. 11 indicates that it is rather difficult to extract Γ_n/Γ_p from the ratio of neutrons to protons N_n/N_p unless this ratio is determined with high

precission. The fact that the relative error of the ratio N_n/N_p is the sum of the relative errors in N_n and N_p, together with the fact that usually neutrons are measured with little precission, makes the uncertainty of this magnitude very large and leads to large errors in Γ_n/Γ_p.

It is clear from the former considerations that the separate number of protons and neutrons per Λ decay would provide more information. The gain is twofold: on the one hand the individual relative errors of N_n and N_p are smaller than for their ratio. On the other hand, one has two pieces of information which will provide two independent bands of allowed values of Γ_n/Γ_p. The intersection of the two bands will give the final allowed region. This procedure should give rise to more precise determinations of Γ_n/Γ_p in the future. For this purpose we present our predictions in Figs. 12 and 13.

In Fig. 12, we show the number of neutrons per Λ decay event, N_n, as a function of Γ_n/Γ_p. From top to bottom the results correspond to detection energy cuts of 0, 30 and 40 MeV. The dashed lines correspond to considering only the 1N induced decay, while the solid line includes also the 2N induced one. The number of protons per Λ decay event, N_p, is shown, as a function of Γ_n/Γ_p, in Fig. 13 with the same meaning as in Fig. 12.

The potential of these two figures to determine Γ_n/Γ_p can be shown with the following example: From Figs. 12 and 13 we see that for $\Gamma_n/\Gamma_p = 0.5$ and $E_{\rm cut} = 30$ MeV we obtain $N_n = 1.28$ and $N_p = 0.62$. Assume now a 10% error in the values of N_n and N_p. From Fig. 12 one obtains the range $\Gamma_n/\Gamma_p = 0.175$—$1.0$, while Fig. 13 gives the range $\Gamma_n/\Gamma_p = 0.35$—0.75. On the other hand, if only the ratio N_n/N_p from Fig. 11 were used, the range of values would be $\Gamma_n/\Gamma_p = 0.2$—0.75. We can therefore see that N_p is more selective than N_n in order to determine Γ_n/Γ_p and also more selective than the ratio N_n/N_p. However, in this particular example we can see that the ratio N_n/N_p is more selective than the number N_n itself. The fact that N_n increases as Γ_n/Γ_p increases, while N_p decreases, makes the ratio N_n/N_p a steeper function of Γ_n/Γ_p than any of the numbers N_n or N_p and helps in getting smaller errors for Γ_n/Γ_p. However, one has the handicap that one must sum the relative errors of N_n and N_p.

With other values and other errors we could have different situations in which the measurements of N_n could give additional information to the one provided by N_p, but the former example indicates that the measurement of N_p is probably the most crutial magnitude in order to determine Γ_n/Γ_p.

Unfortunately the experiment of Ref. [5] does not provide the number of decay events corresponding to the total number of neutrons and protons measured and therefore, only the ratio can be used in our analysis. On the other hand, the work of Ref. [6] contains a spectrum of protons but it is conditioned by several cuts, efficiencies and geometries of the detectors, and does not allow the extraction of N_p nor can it be compared to the spectrum which we have calculated. However, the determination of N_p is one of the aims of the collaboration in Ref. [27] in the near future. As hinted by our observation above, the determination of N_p alone can provide as much information as the combined measurement of N_n and N_p. As we have shown, precise measurements of N_p with different cuts, which can be done if the spectrum of protons is also known, would provide reliable values for Γ_n/Γ_p.

V. CONCLUSIONS

We have evaluated the spectrum of neutrons and protons following the decay of Λ hypernuclei. For this purpose we calculated the momentum distribution of the nucleons coming from the one nucleon induced and two nucleon induced Λ decay. Final state interaction of the nucleons was also considered using a Monte Carlo computer simulation technique, successfully applied to other physical processes. By integrating over the energy spectrum we can also obtain the number of neutrons and protons for any energy cut in the nucleon detectors. We have seen that the measurement of N_n and N_p, the number of neutrons and protons per Λ decay, can be used to determine the ratio Γ_n/Γ_n reliably. We observed that the value of N_p was more selective in determining the value of Γ_n/Γ_p than N_n or the ratio N_n/N_p, and this should serve as a guideline for future experiments.

The two nucleon induced Λ decay channel was found relevant in the analysis. Even if

the fraction of this decay channel is only 30% of the free Λ width, or 20% of the total Λ width in the nucleus [13], it has some repercussion in the determination of Γ_n/Γ_p and, as a consequence, enlarges the error band for Γ_n/Γ_p, obtained from given values of N_n/N_p, with respect to a determination omitting this channel in the analysis. Even then, the ratio Γ_n/Γ_p can be determined reliably provided one can measure N_p and N_n (particularly N_p) with sufficient precission.

The analysis done here, and the figures presented, will allow a direct determination of Γ_n/Γ_p from future measurement of N_n and N_p, which in view of the results obtained here should be encouraged.

ACKNOWLEDGMENTS

We would like to acknowledge useful discussions with A. Gal, H. Ejiri, O. Hashimoto, T. Kishimoto, J. Nieves and M. Oka. This work has been partly supported by DGICYT contracts AEN 93-1205, PB92-071 and by the European Union contract No. CHRX-CT 93-0323.

REFERENCES

[1] K. Tacheuchi, H. Takaki and H. Bando, Prog. Theor. Phys. **73**, 841 (1985).

[2] J. Dubach, Nucl. Phys. **A450**, 71c (1986).

[3] E. Oset, P. Fernández de Córdoba, L.L. Salcedo and R. Brockmann, Phys. Rep. **89**, 79 (1990).

[4] A. Montwill et al. Nucl. Phys. **A234**, 413 (1974).

[5] J.J. Szymansky et al. Phys. Rev. C **43**, 849 (1991).

[6] H. Noumi et al., Phys. Rev. C **52**, 2936 (1995).

[7] C. Bennhold, A. Parreño and A. Ramos, Few Body Systems Suppl. **9**, 475 (1995). A. Parreño, A. Ramos and C. Bennhold, Univ. of Barcelona preprint.

[8] M. Shmatikov, Nucl. Phys. **A580**, 538 (1994).

[9] K. Itonaga, T. Ueda and T. Motoba, Nucl. Phys. **A585**, 331c (1995); ibid, Proc. of the WEIN 95 Conference, H. Ejiri, T. Kishimoto and T. Sato Eds., World Scientific 1995, p. 546.

[10] C. Y. Cheung, D.P. Heddle and L.S. Kisslinger, Phys. Rev. C **27**, 335 (1983).

[11] T. Inoue, S. Takeuchi and M. Oka, Nucl. Phys. **A597**, 563 (1996).

[12] W. Alberico, A. de Pace, M. Ericson and A. Molinari, Phys. Lett. **B256**, 134 (1991).

[13] A. Ramos, E. Oset and L.L. Salcedo, Phys. Rev. C **50**, 2314 (1994).

[14] A. Gal, in Proc. of the WEIN 95 Conference, H. Ejiri, T. Kishimoto and T. Sato Eds., World Scientific 1995, p. 573.

[15] E. Oset and L.L. Salcedo, Nuc. Phys. **A443**, 704 (1985).

[16] K. Itonaga, T. Motoba, and H. Bando, Z. Phys. **A330**, 683 (1988).

[17] T. Motoba, Nucl. Phys. **A527**, 485c (1991); Few Body Systems Suppl. **5**, 386 (1992); Nucl. Phys. **A547**, 115c (1992).

[18] J. Nieves and E. Oset, Phys. Rev. C **47**, 1478 (1993).

[19] U. Straub, J. Nieves, A. Faessler and E. Oset, Nucl. Phys. **A556**, 531 (1993) 686.

[20] R.C. Carrasco, E. Oset and L.L. Salcedo, Nuc. Phys. **A541**, 585 (1992).

[21] R.C. Carrasco, M.J. Vicente-Vacas and E. Oset, Nucl. Phys. **A570**, 701 (1994).

[22] A.L. Fetter and J.D. Walecka, Quantum Theory of Many Particle Systems (McGraw-Hill, N.Y. 1971).

[23] L.L. Salcedo, E. Oset, M.J. Vicente Vacas and C. Garcia-Recio, Nucl. Phys. **A484**, 557 (1988).

[24] E. Oset and W. Weise, Nuc. Phys. **A319**, 477 (1979).

[25] J. Cugnon, private communication.

[26] G. Franklin, private communication.

[27] O. Hashimoto, private communication.

FIGURES

FIG. 1. Λ self-energy diagrams for the one nucleon induced channel from Refs. [13,15]. The dotted line cuts the states which are placed on shell in the evaluation of $Im\,\Sigma$.

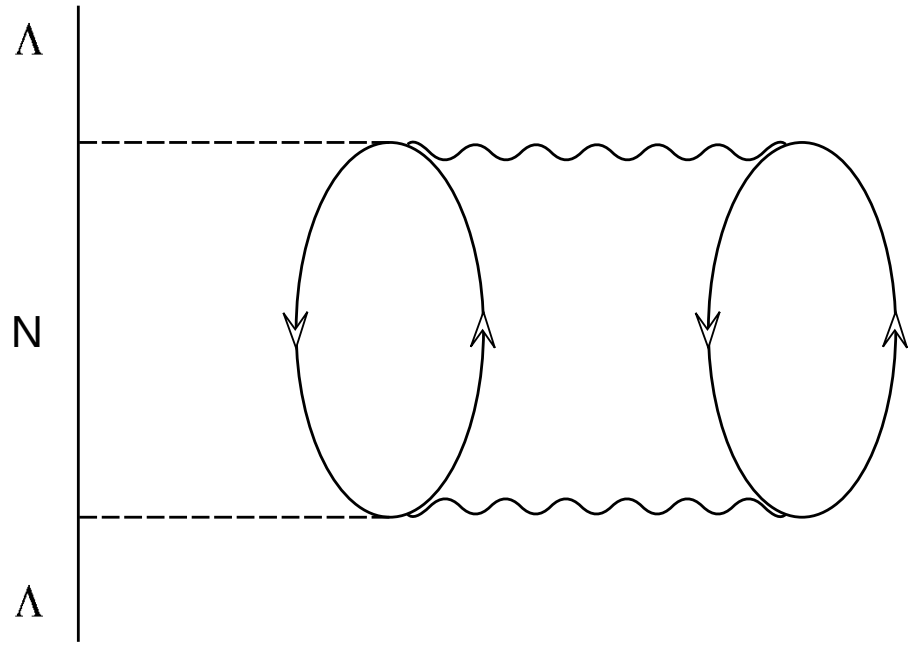

FIG. 2. Λ self-energy diagram for the 2N induced Λ decay mechanism from Ref. [13].

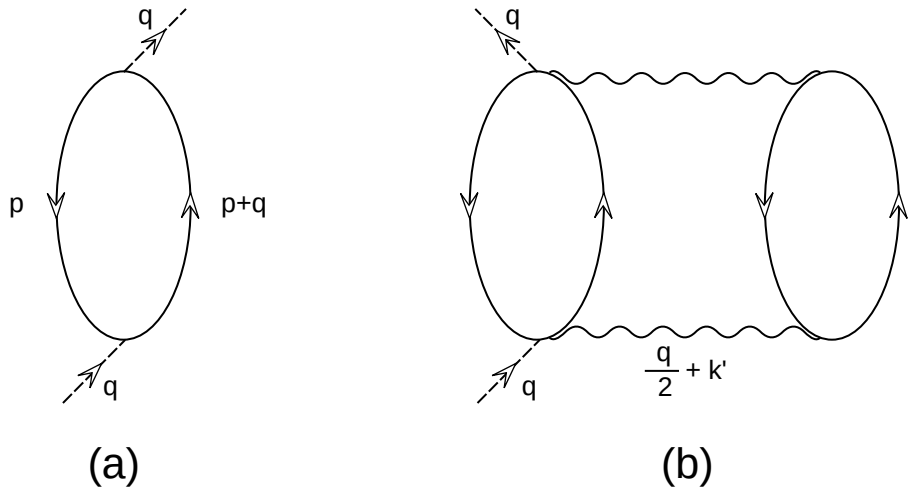

FIG. 3. Diagrams employed in the evaluation of $Im\,\overline{\Pi}^{*}_{\rm 1p1h}$ (a) and $Im\,\overline{\Pi}^{*}_{\rm 2p2h}$ (b).

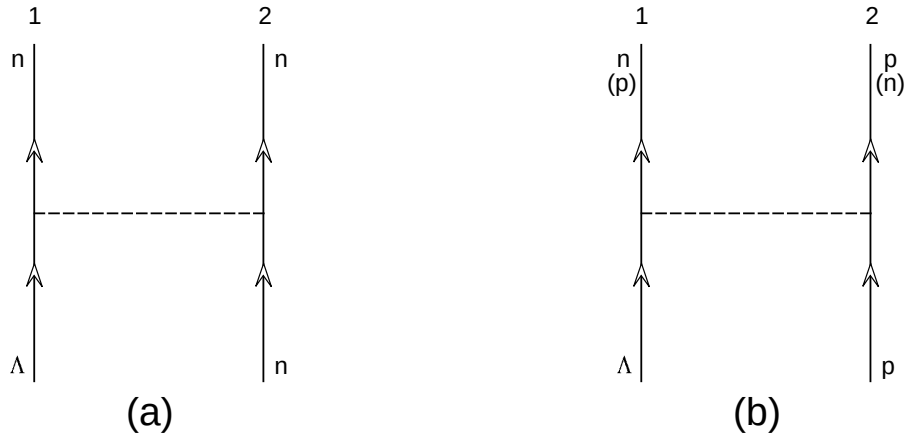

FIG. 4. Feynman diagrams for the transition $\Lambda N \to NN$: neutron induced Λ decay (a) and proton induced Λ decay (b).

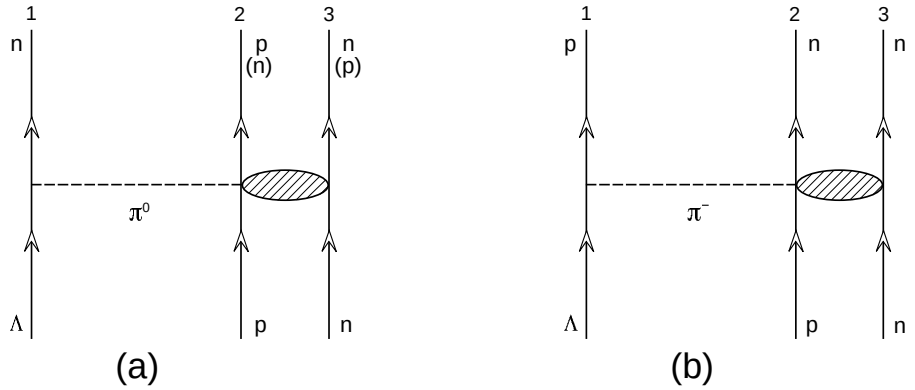

FIG. 5. Feynman diagrams for the two nucleon induced Λ decay through virtual π^0 absorption (a) and virtual π^- absorption (b).

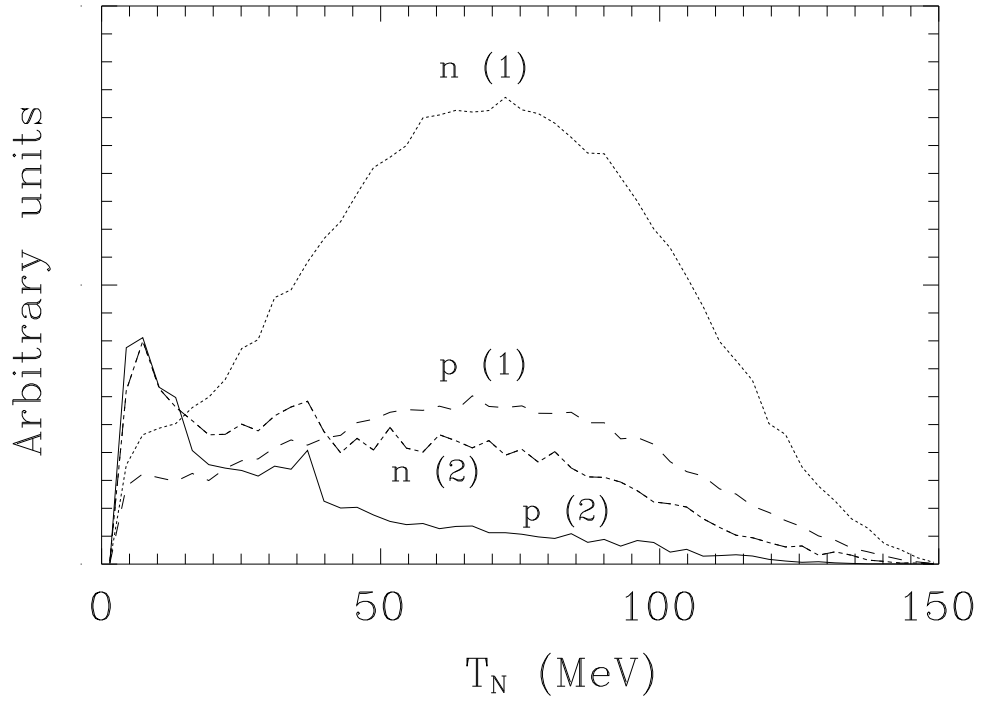

FIG. 6. Spectra of neutrons and protons in the decay of $^{12}_{\Lambda}$C. Dashed line: protons from the 1N induced mechanism. Dotted line: neutrons from the 1N induced mechanism. Solid line: protons from the 2N induced mechanism. Dash-dotted line: neutrons from the 2N induced mechanism. The results have been obtained for a value $\Gamma_n/\Gamma_p = 1$.

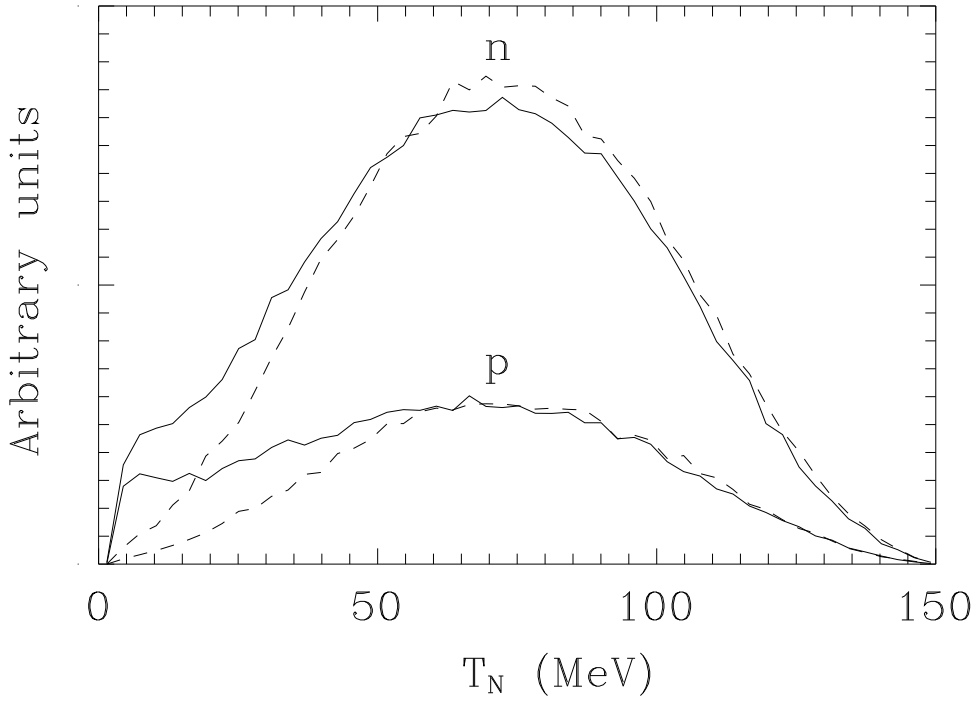

FIG. 7. Effect of the final state interactions in the spectrum of nucleons emitted in the 1N induced decay. Dashed line: results without FSI. Solid line: results including FSI.

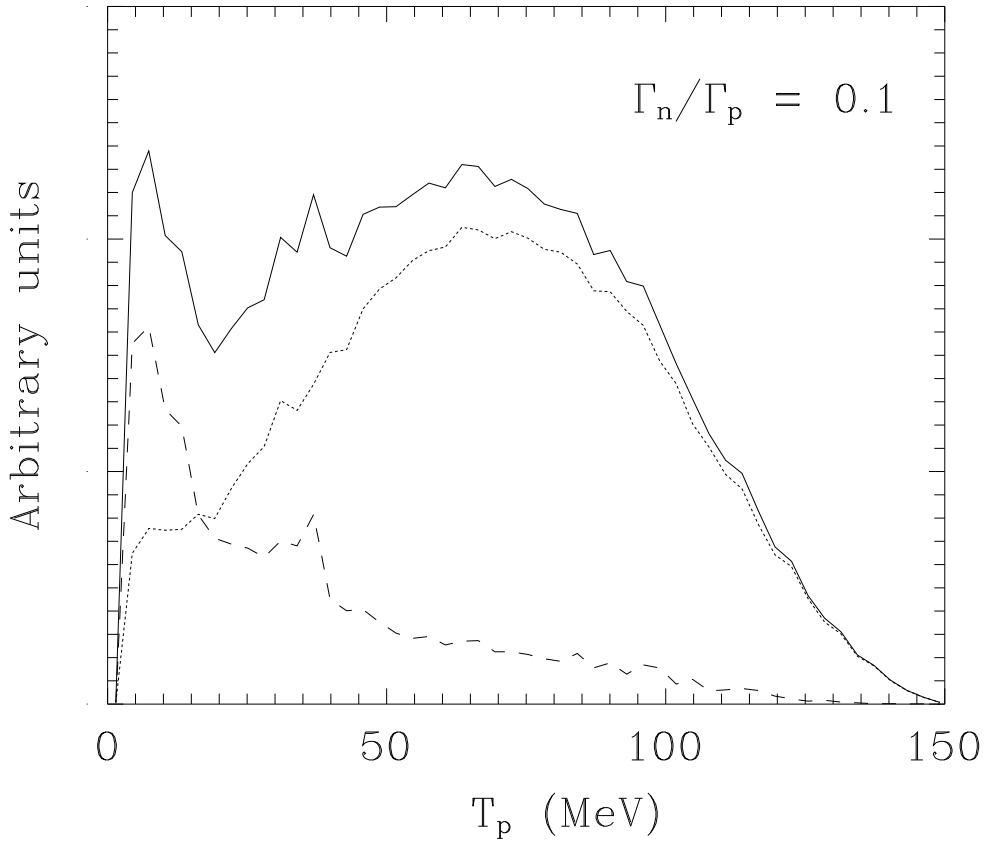

FIG. 8. Proton spectrum obtained for a value $\Gamma_n/\Gamma_p = 0.1$. Dotted line: 1N induced mechanism. Dashed line: 2N induced mechanism. Solid line: Total.

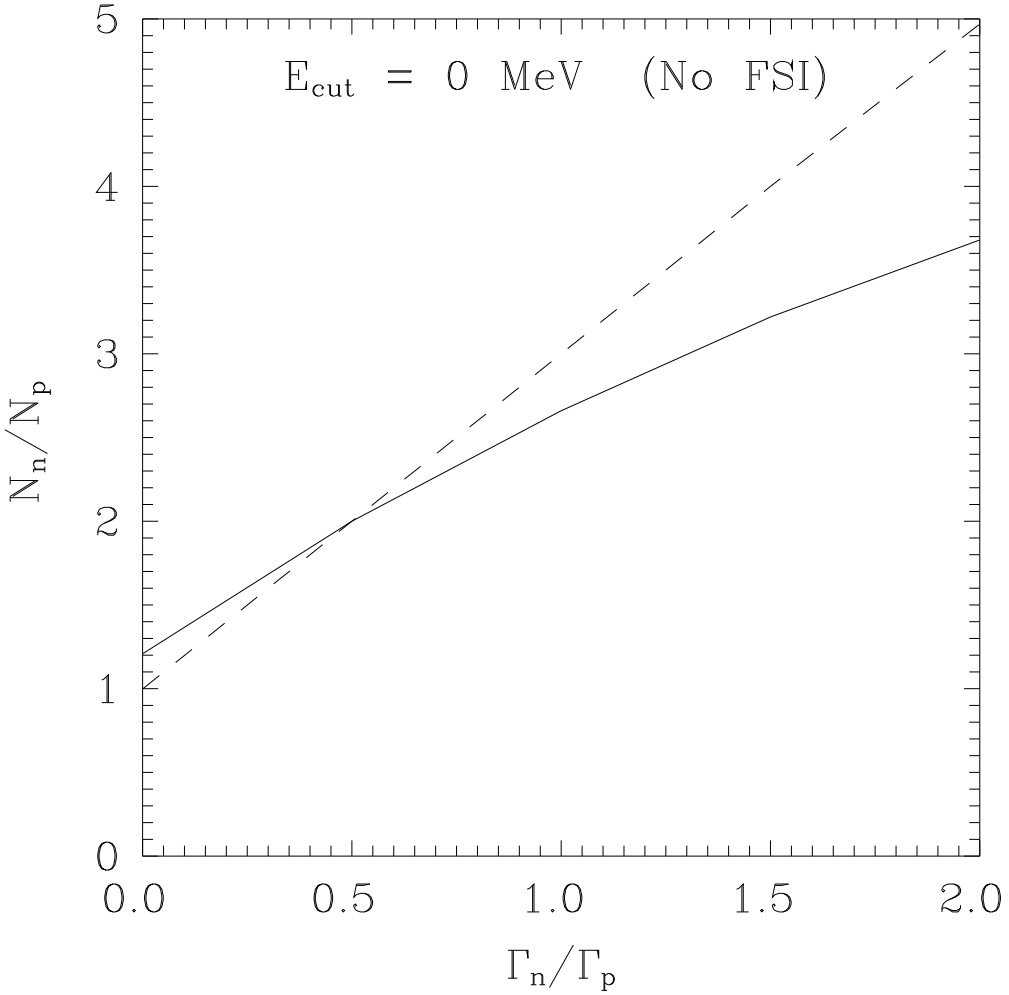

FIG. 9. N_n/N_p as a function of Γ_n/Γ_p with no cut in the detection energy and no final state interactions. Dashed line: 1N induced mechanism. Solid line: 1N + 2N induced mechanisms.

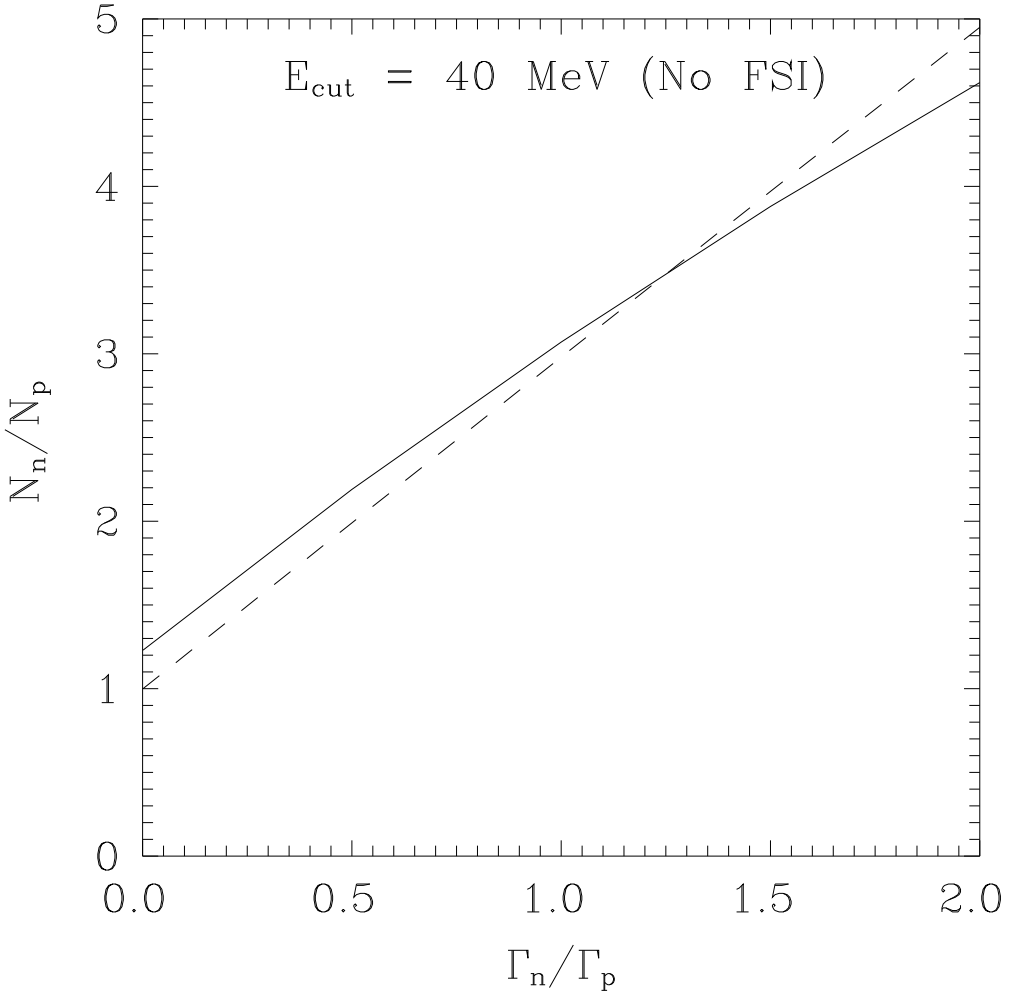

FIG. 10. Same as Fig. 9, but with a detection threshold of 40 MeV and no final state interactions.

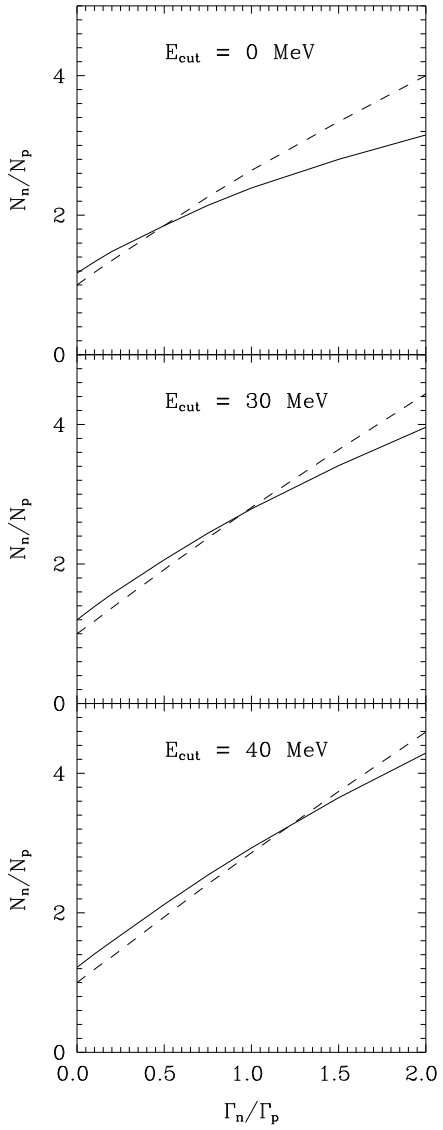

FIG. 11. N_n/N_p as a function of Γ_n/Γ_p including final state interaction effects and applying energy cuts of 0, 30 and 40 MeV. Dashed line: 1N induced mechanism. Solid line: 1N + 2N induced mechanisms.

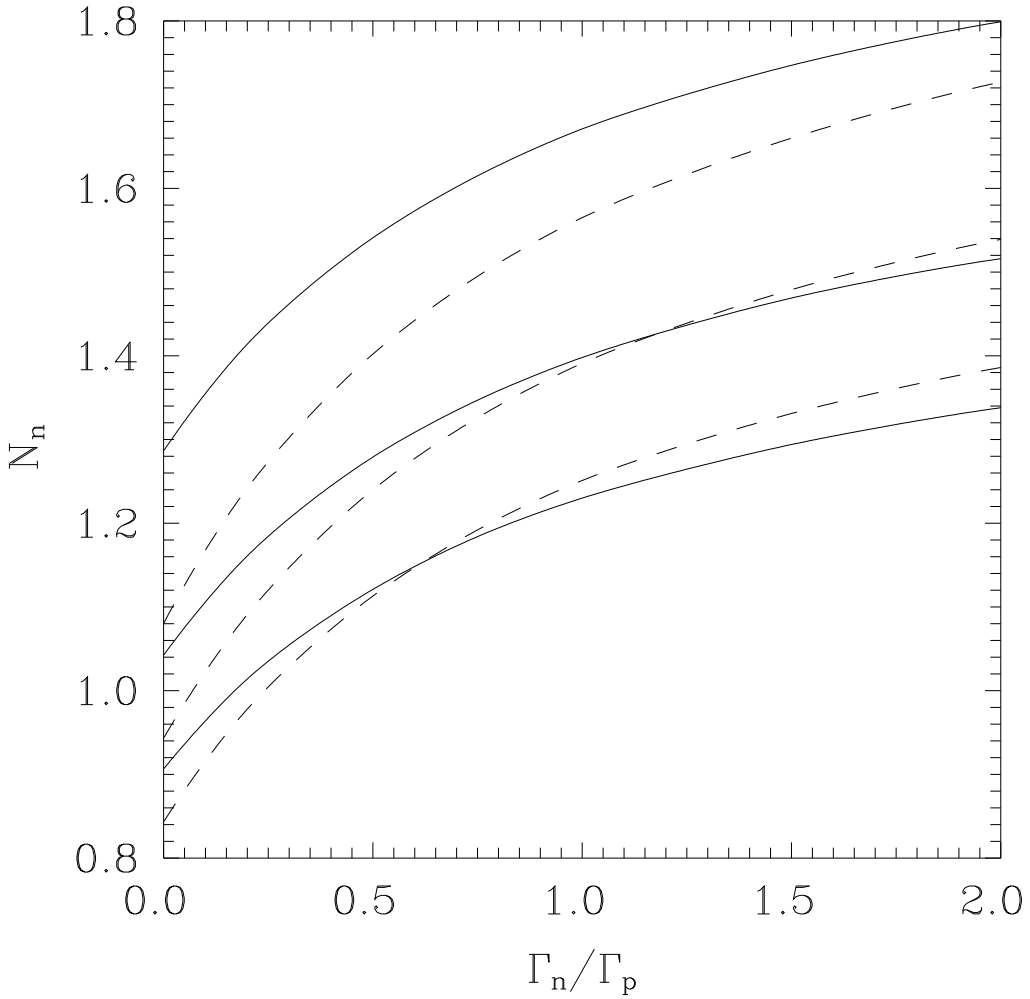

FIG. 12. Number of neutrons per Λ decay as a function of Γ_n/Γ_p. Dashed lines: 1N induced mechanism. Solid lines: 1N + 2N induced mechanism. Final state interactions are considered and, from top to bottom, the results include energy cuts of 0, 30 and 40 MeV, respectively.

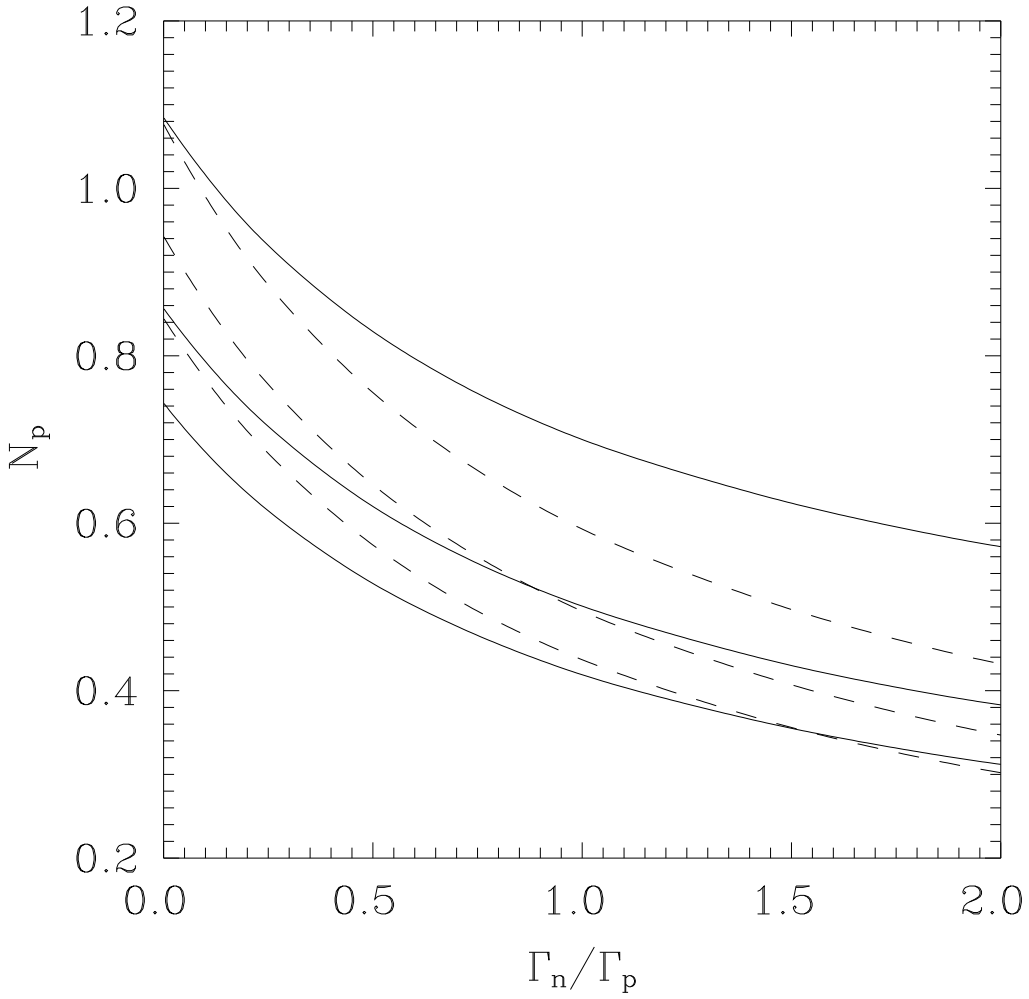

FIG. 13. Same as Fig. 12 for the number of protons per Λ decay.